JOURNAL	Fullerenes, Nanotubes and Carbon Nanostructures
CITATION	Eken, T. Y., Kaykilarli, C., Tuna, A., Şam Parmak, E. D., Uzunsoy, D., & Peljo, P. (2025). Graphene nanoplatelet-coated electrodes with cellulose binders for 4-hydroxy-2,2,6,6-tetramethylpiperidine 1-oxyl-based aqueous posolyte. *Fullerenes, Nanotubes and Carbon Nanostructures*, *33*(8), 778–789.
DOI	https://doi.org/10.1080/1536383X.2025.2458510

Graphene Nanoplatelet-Coated Electrodes with Cellulose Binders for 4-Hydroxy-2,2,6,6-Tetramethylpiperidine 1-oxyl-Based Aqueous Posolyte

Taha Yasin Eken,[1,2*] Cantekin Kaykılarlı,[1] Ali Tuna,[2] Ebru Devrim Şam Parmak,[1] Deniz Uzunsoy,[1] Pekka Peljo[2*]

[1] Department of Metallurgical and Materials Engineering, Faculty of Engineering and Natural Science, Bursa Technical University, TR-16310 Bursa, Türkiye
[2] Department of Mechanical and Materials Engineering, Faculty of Technology, University of Turku, FI-20014 Turku, Finland

[*]corresponding author´s email: yasin.eken@btu.edu.tr, pekka.peljo@utu.fi

Abstract

This study investigates the development of cellulose-bonded graphene nanoplatelet-coated electrodes for organic flow batteries (OFBs) utilizing 4-Hydroxy-2,2,6,6-Tetramethylpiperidine 1-oxyl (TEMPOL) as the active material. Graphite felt electrodes were coated via an optimized dip-coating process, varying the number of dips (1, 5, and 10). Cyclic voltammetry (CV) showed a 150% increase in oxidation peak current and a 250% increase in reduction peak current for the 10-dipped electrodes compared to pristine ones. Electrochemical impedance spectroscopy (EIS) revealed a 35% reduction in charge transfer resistance (R_p) for the 5-dipped electrodes, indicating enhanced ion transfer efficiency. Surface characterization analyses, including SEM, XRD, and Raman spectroscopy, confirmed uniform graphene coatings and structural integrity, while contact angle measurements demonstrated a transition from hydrophobic (157°) to hydrophilic (0°) surfaces, improving wettability and electrolyte interaction. These findings establish cellulose as a sustainable, cost-effective binder, with potential scalability for large-scale energy storage applications.

Keywords: Organic Flow Batteries, Graphene, Dip Coating, CV, EIS

Introduction

Organic flow batteries (OFBs) are a promising technology for large-scale and long-duration energy storage [1–3]. They utilize organic compounds as the active material and are known for their high energy density, flexibility in design, and low cost. The unique characteristics of OFBs make them a highly promising technology for large-scale and long-duration energy storage, making them an area of active research and development. During the global energy transition, OFBs have emerged as an important storage alternative, offering versatile solutions to address the increasing challenges of energy storage and distribution. OFBs can be preferred in various sectors, such as renewable energy integration, grid stabilization, and off-grid applications, where the demand for reliable and efficient energy storage solutions continues to escalate [4,5].

Electrodes are important components of OFBs, and their performance affects the overall efficiency of the battery [6–8]. They act as the interface where the electrochemical reactions take place, facilitating the flow of electrons and ions during charge and discharge cycles. Also, they provide active sites for electrochemical reactions, and influence power performance and energy efficiency. In the OFBs, the electrodes are surrounded by electrolytes, enhancing their functionality. The most common electrode used for OFB applications are graphite felts due to their high porosity, high mechanical strength, and electrical conductivity properties. Various materials are currently under investigation to enhance the performance of graphite electrodes [9,10]. High aspect ratio carbon elements like carbon nanotubes and graphene flakes are utilized in electrode active layers to improve electrical conductivity and mechanical stability. These advancements in electrode design and materials contribute significantly to the efficiency and performance of flow batteries, making them essential components for various energy storage systems, including other flow battery types [11,12].

Despite significant advancements in OFBs, challenges persist in achieving cost-effective and environmentally sustainable solutions for large-scale applications. Current research predominantly focuses on improving electrolyte formulations, with less emphasis on the design and optimization of electrodes. Many studies investigate the use of popular organic active materials such as TEMPO [13,14], often paired with Nafion [10] as a binder due to its proven performance. However, high cost Nafion and environmental limitations hinder its scalability for industrial applications.

Additionally, some research explores the use of alternative additives to modify electrode surfaces, such as nickel chloride [15], high-temperature etching method and then carbon nanoparticles [13], or heteroatom-doped graphite felt [14] materials, but these approaches often fail to balance performance with sustainability. In this context, graphene, a two-dimensional carbon material, has emerged as a highly promising candidate since it exhibits exceptional electrical conductivity, mechanical strength, and chemical stability [16]. Its unique structure and large surface area allow for efficient electron transfer and enhanced electrochemical reactions within the OFB system. Properties and applications of graphene has been extensively researched, particularly in electronics, flow batteries, fuel cells, supercapacitors, batteries, photovoltaic devices, and more, highlighting its potential to revolutionize various domains of life [17]. The preparation, tailoring, and modification techniques for graphene have been continuously developed to optimize its properties for diverse applications, emphasizing its versatility and adaptability in different fields especially for flow batteries [18–21].

Various binding agents or matrix materials are used for graphene-graphite binding in the literature [22]. Nafion, Polyvinyl alcohol (PVA), Polymethyl methacrylate (PMMA), and polymeric resins are some of the well-known binders used for this purpose [23]. Cellulose is a natural polymer that also serves as an effective binder for graphene and graphite materials. It has been extensively studied as a binding agent for graphene and graphite materials due to its exceptional compatibility [24]. The combination of cellulose with graphene has shown significant improvements in mechanical strength and stability of composite structures. The synergistic effects of cellulose and graphene contribute to the improved adhesion between

graphene layers, leading to enhanced mechanical properties and stability in the resulting materials. Its remarkable compatibility with graphene and graphite makes it a commonly employed binding material [25]. The inclusion of cellulose-based binders enhances the adhesion between the layers of graphene and graphite, resulting in improved mechanical strength and overall stability. For the coating purposes, cellulose and graphite are used with dip coating processes. Although the use of Nafion has advantages such as chemical stability, mechanical strength, and good proton conductivity in fully humidified conditions, there are a number of important limitations and problems. Nafion® incurs high production costs, mainly attributed to the fluorination process of polyethylene to PTFE. The structural issue arises from a significant reduction in mechanical integrity attributed to its low glass transition temperature (120–140 ◦C). The elevated fluorine content in Nafion raises environmental concerns. Nafion® is classified as a per- and polyfluoroalkyl substance (PFAS), recognized for its significant environmental persistence. The strength of the carbon-fluorine covalent bond hinders complete degradation, resulting in the bioaccumulation of these materials. PFASs, owing to their water solubility and mobility, can contaminate soils and water upon release into the environment, thereby potentially threatening human health and ecosystems. Consequently, governments are increasingly establishing regulations that limit the use of specific PFAS compounds [26]. Cellulose is both biodegradable and biocompatible, and it can be derived from several renewable sources, such as agricultural waste and recycled paper pulp [27].

Cellulose is a recognized natural biopolymer that offers numerous benefits, including affordability, renewability, ease of processing, biodegradability, and favorable mechanical properties, dielectric characteristics, piezoelectricity, and convertibility. Cellulose is the most prevalent and recognized natural biopolymer, present in several plants and also biosynthesized by specific microorganisms. It has been extensively utilized in the production of printing paper, packaging, textiles, healthcare items, and medicines. Cellulosic materials are useful due to their chemical distinctiveness, shape adaptability, ease of production, mechanical strength, and biodegradability [28]. Cellulose is both biodegradable and biocompatible, and it can be derived from several renewable sources, such as agricultural waste and recycled paper pulp [27].

Dip coating plays a crucial role in enhancing the performance of graphene nanoplatelet-coated electrodes with cellulose binders for OFBs. The dip coating process significantly affects the electrochemical activity of electrodes [29]. Moreover, the utilization of cellulose as binders in conjunction with graphene flakes leads to the development of high-performance organic nanohybrid electrodes, ensuring superior cycle stability and areal capacity. Additionally, the unique ability of cellulose to disperse carbon-rich materials contributes to improved mechanical and electrochemical performance in battery applications. These findings highlight the importance of dip coating techniques and the synergistic effects of graphene and cellulose nanofibers in optimizing the performance of electrodes for OFBs.

4-hydroxy-2,2,6,6-tetramethylpiperidin-1-oxyl (TEMPOL) is a promising posolyte for OFB studies due to its high solubility, stability, and favorable electrochemical properties. However, literature on the use of TEMPOL in conjunction with graphene nanoplatelet-coated electrodes focused on thermal modifications [13,30].

This study presents a novel approach to enhancing OFB electrodes by combining graphene nanoplatelets with cellulose, a sustainable and biodegradable binder. Unlike conventional methods that rely on costly and environmentally challenging materials like Nafion, this study explores the potential of cellulose to provide a scalable, cost-effective, and high-performance alternative. By utilizing a dip-coating process [31], we demonstrate significant improvements in electrochemical performance, wettability, and structural integrity. To our knowledge, this is the first study to investigate the integration of cellulose as a binder in graphene-coated electrodes for TEMPOL OFBs, bridging the gap between sustainability and scalability in advanced energy storage systems.

Materials and Method

Materials

Cellulose, DMF (N,N-dimethylformamide) and NMP (N-methyl-2-pyrrolidone) were supplied by Sigma Aldrich and graphene powders were supplied by Nanografi company. Ouzheng brand OZ0130 model polyacrylonitrile (PAN) based carbon felts (thickness: 5 mm, carbon content >99%) were used as graphite felts.

Coating Process

Dip coating method was applied with a similar method previously done [31]. For this purpose, carbon felts were cut to size 25x20 mm. Then the solution was prepared. While preparing the solution, 100 mg cellulose was dissolved in 200 mL DMF. Then, 225 mg of graphene powder was added to the prepared mixture. Finally, this prepared mixture was dissolved in 450 mL NMP. After mixing in a magnetic stirrer for 24 hours and 600 steps/second, the coating process was started. Graphite felt electrodes were dip-coated by immersing them into the prepared solution for 5 seconds per dip, with the number of dips varying between samples. After coating, the electrodes were dried in an oven at 120 °C for 6 hours. The coating process is shown in Figure 1 (a).

Electrochemical Studies

Electrochemical tests were carried out with a CHI608E (CH Instruments, Inc., Austin, TX). CV and EIS techniques were used. Aftermath software (Pine Research, Durham, NC/USA) was used for EIS analyses. CV behaviors of the electrodes were studied in an aqueous solution of 1 mM TEMPOL with 1 M NaCl supporting solution throughout a potential range of 0 to 1 V. The electrochemical impedance spectra of the electrodes were measured using a typical three-electrode system at an open circuit potential in the frequency range of $1 – 10^5$ Hz. The working electrodes were platinum wire knitted graphite felts (surface area 7.25 cm^2), whereas the reference and counter electrodes were Ag/AgCl (3 M KCl) and Pt electrodes. N_2 gas was purged during the CV tests. All CV experiments were executed at room temperature. Figure 1 (b) showed the 3-electrode cell and potentiostat system with electrodes. The knitted graphite felt also was shown as a small picture in this figure.

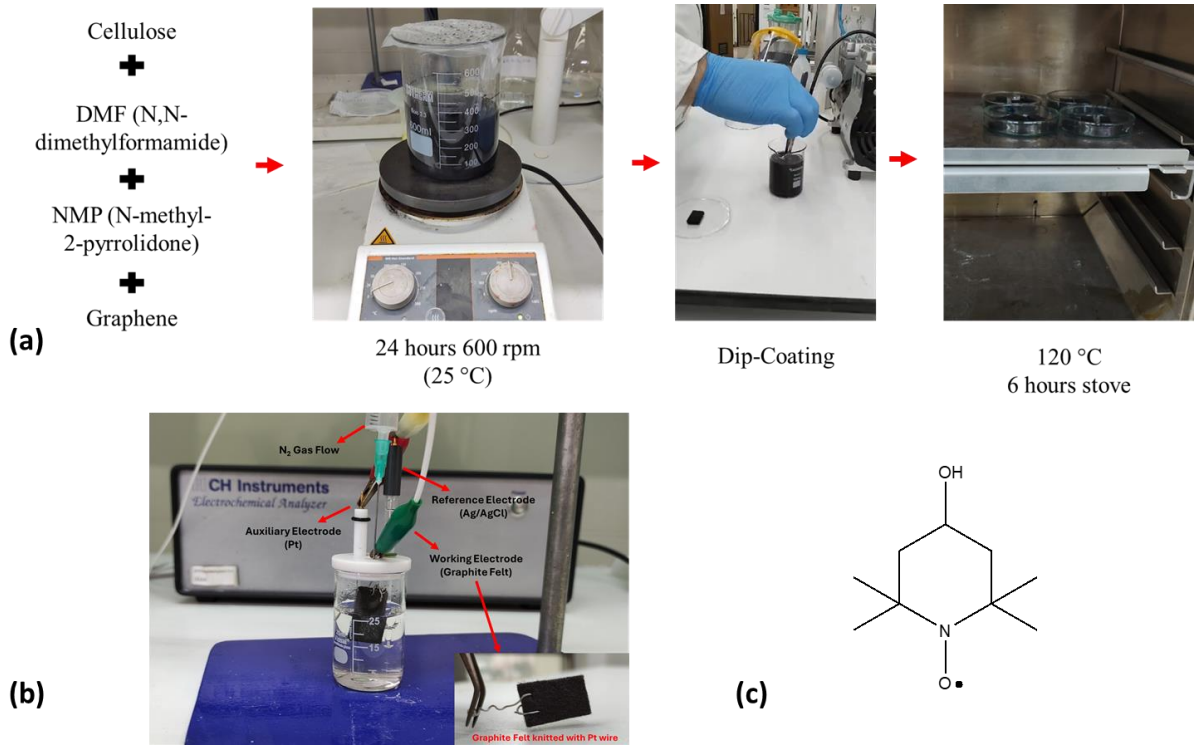

Figure 1. (a) The dip-coating process. (b) The 3-electrode system used for electrochemical tests in this study. Graphite felts were used as working electrodes. Felts were knitted with a platinum wire for conductivity. 1 mM TEMPOL solution was used as electrolyte. Tests were performed at room temperature and nitrogen atmosphere. (c) The molecular chemical structure of TEMPOL.

Synthesis of TEMPOL

To a 25 mL two-necked round bottom flask, 2,2,6,6-tetramethylpiperidin-1-oxyl, 1.563 g, 10 mmol) in toluene (10 mL) was added. The reaction mixture was heated up to 40°C for 30 minutes and then $FeSO_4.7H_2O$ (210 mg, 750 µmol) as a Fenton reaction catalyst was added to the solution. After stirring for 15 minutes, 50% H_2O_2 (5 mL) was added dropwise. The mixture was stirred for additional 3 hours. Once the reaction is completed, the catalyst was filtered off. The solution was evaporated, and the crude was dissolved in a minimum amount of 20% v/v hexane in acetone) and left to stand in refrigerator at -20°C for 16 hours. The reddish-orange colored crystalline solid was filtered over Büchner funnel, washed with hexane, and dried under reduced pressure to give 1.120 g of 4-hydroxy-2,2,6,6- tetramethylpiperidin-1-oxyl (yield: ~65%). The molecular chemical structure of TEMPOL is given in Figure 1 (c). The obtained solid was characterized by EPR, FTIR, and CV (CHI608E, CH Instruments, TX/USA) techniques.

The EPR and FTIR spectra of TEMPOL are given in Figure 2**Hata! Başvuru kaynağı bulunamadı.** (a) and **Hata! Başvuru kaynağı bulunamadı.**(b) respectively. The FTIR peaks of TEMPOL is listed as Table 1**Hata! Başvuru kaynağı bulunamadı.**. In the EPR, it is observed that the TEMPOL radical molecule has a ‘three peak’ structure which is attributed to hyperfine splitting. In this case, it arises as a result of the unpaired electron in the oxygen of

the TEMPO radical molecule and the neighboring nitrogen nucleus which can adopt a nuclear spin of (I = 1). From this interaction, there are three different and possible spin states for the nitrogen nucleus such as m_I = +1, 0, -1 that causes the EPR signal to split into three peaks. The number of peaks observed is a reflection of the hyperfine coupling constant which describes the degree of interaction between nitrogen and the unpaired electron. The distance between the peaks on the EPR spectrum is a function of this coupling constant. Furthermore, the location and strength of these peaks could elucidate the local geometry and motion of the TEMPOL radical since a change in the spectrum may arise from a changed molecular environment or molecular interaction. TEMPOL is water-soluble and EPR spectrum was obtained in aqueous solution of TEMPOL. In FTIR spectrum, most importantly, around sharp 3400 cm^{-1}, O-H stretch can be seen which is related to attached hydroxyl group into the non-aromatic ring system. Between 3000-2800 cm^{-1}, multiple C-H stretch can be observed which indicates the ring system. Around 1360 cm^{-1} and 990 cm^{-1}, the N-O stretching and bending can be observed respectively. Together with EPR spectrum this N-O stretching and bending can be understood as radical behavior for TEMPOL. All these observations are different from the starting material TEMPO, but the TEMPOL compound is water soluble. CV test of 5 mM TEMPOL in 1 M NaCl using glassy carbon electrode was done and given in Figure 3**Hata! Başvuru kaynağı bulunamadı.** (a). The redox mechanism is given in Figure 3**Hata! Başvuru kaynağı bulunamadı.** (b). This voltammogram shows a typical CV behavior of TEMPOL in neutral conditions**.**

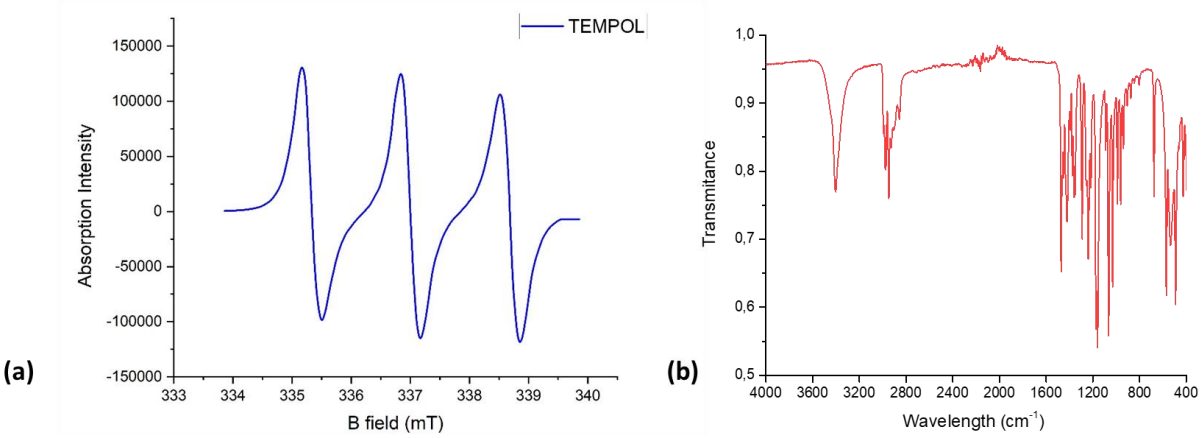

Figure 2. (a) EPR and (b) FTIR spectrum of TEMPOL.

Table 1. The FTIR peaks, bond type and vibration type of TEMPOL molecule.

peak	bond type	vibration type
3404 (s)	O-H	stretch
2949 (m)	C-H (CH_3, CH_2, CH)	stretch
1472 (m)	C-H (CH_2)	bending
1421 (m)	C-H (CH_3)	bending
1362 (m)	N-O	stretch
1292 (m)	C-O	stretch
1240 (m)	C-N	stretch
1067 (m)	C-C	bending

991 (m)	N-O	bending
962 (m)	C-H (CH_2)	rocking
677 (s)	C-H (CH_3)	rocking
571 (s)	C-C	bending
536 (br)	O-H	bending
492 (s)	C-N	bending
428 (s)	C-O	rocking

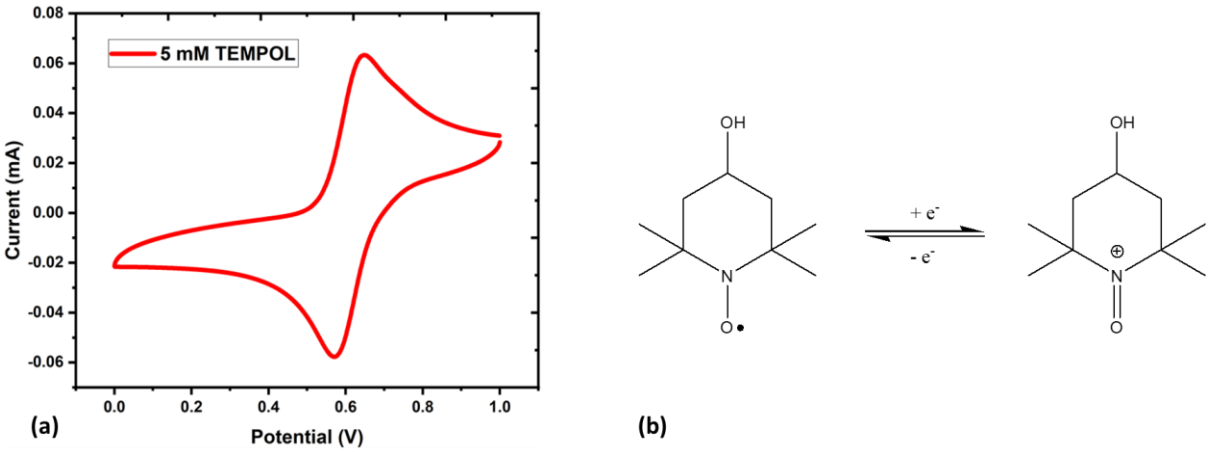

Figure 3. (a) The CV of TEMPOL (WE: 3 mm GC, CE: 0.5 mm Pt wire, RE: 3 M Ag/AgCl in 3 M KCl solution). (b)The redox reaction of TEMPOL/TEMPOL$^+$.

Characterizations

Surface characterizations were performed using scanning electron microscopy (SEM). For SEM tests, samples were gold coated with a Leica EM ACE600 (Leica Microsystems Inc., Germany) device. Gold-coated electrodes were examined with the secondary electron back reflection method at different magnifications using a Zeiss Gemini 300 (Zeiss Gruppe, Oberkochen, Germany) device. Graphene characterization was done using Raman spectroscopy with Renishaw inVia Raman Microscope (Renishaw Plc, Wootton-under-Edge, UK). X-ray diffraction (XRD) analysis was done see the effect of graphene coating. XRD tests were carried out using a Bruker D8 Advance (Bruker Inc., Germany) device between 10° and 90° and a scanning rate of 3°/min. Contact angle tests was applied to see the effect of graphene on wettability properties of graphite felts. Attension Theta (Biolin Scientific Ltd., Sweden) device was used for contact angle tests.

Results

Cyclic voltammetry Analyses after coating

CV analysis was performed to assess the electrochemical performance of pristine, 1-dipped, 5-dipped, and 10-dipped electrodes in 1 mM TEMPOL with 1 M NaCl solution. As shown in Figure 4, oxidation peaks appeared between 0.6–0.9 V and reduction peaks between 0.3–0.6 V (vs. Ag/AgCl). The graphene-coated electrodes exhibited significantly enhanced oxidation and reduction peak currents compared to the pristine electrodes, indicating improved redox activity.

The log (i_p) vs log (v) graph is also shared in Figure 4 (c). It is clearly shown that the most oxidation and reduction peak current values for all scan rates from 5 mV/s to 750 mV/s. The electrodes with 10 dips exhibited the highest electrochemical activity, with distinct oxidation peaks observed. This indicates efficient electron transfer and redox reactions, attributed to the enhanced surface area and conductivity provided by the graphene coating. Compared to the pristine electrodes, the graphene-coated electrodes demonstrated significantly higher current peak values. Specifically, the oxidation peak current increased by 10 times (from 0.31 mA to 3.1 mA) and the reduction peak current by 6.6 (from -0.5 mA to 3.3 mA). In previous studies, increasing the amount of graphene has been shown to enhance the oxidation and reduction peaks observed in CV tests [19,23]

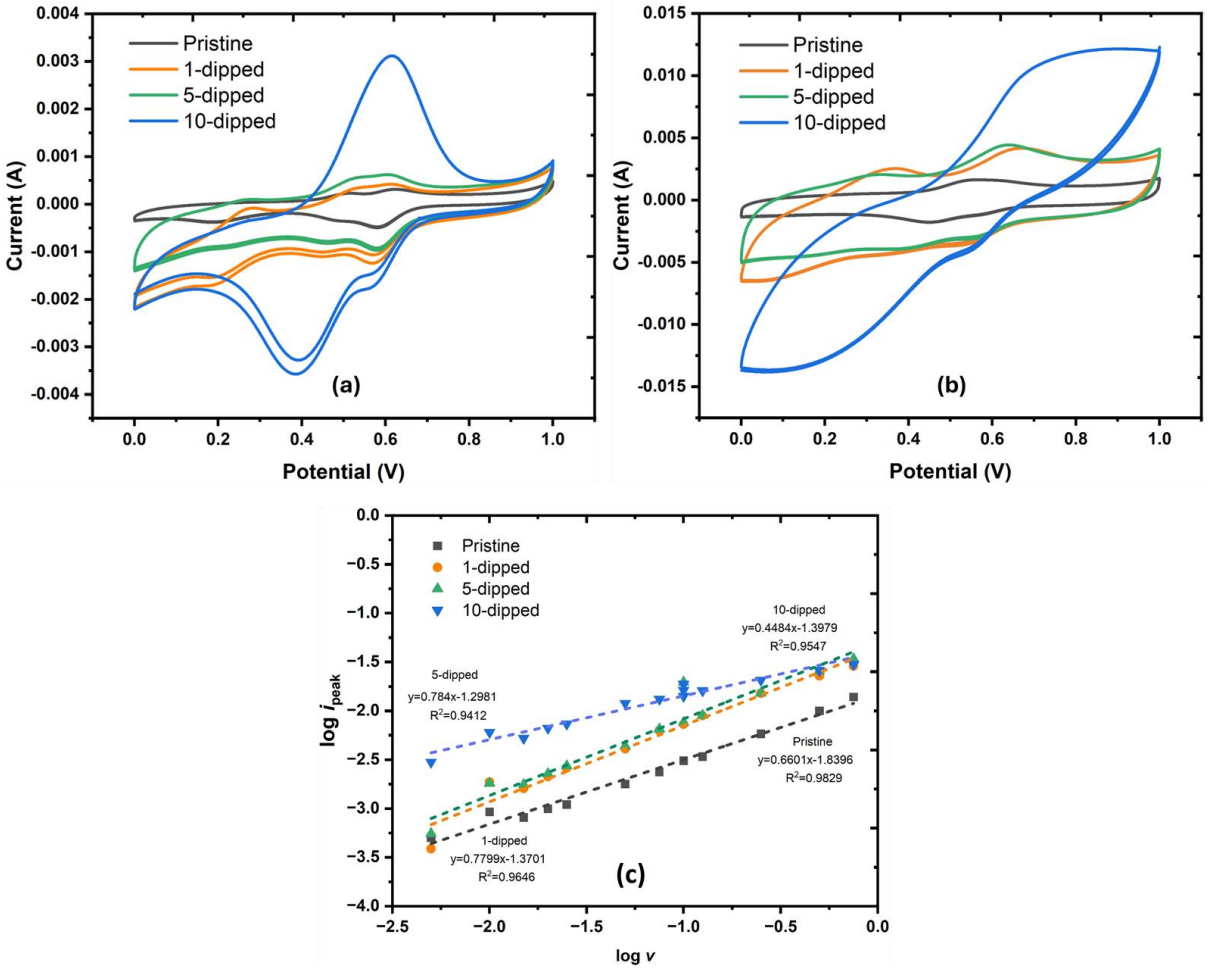

Figure 4. *CV curves of pristine, 1-dipped, 5-dipped, and 10-dipped electrodes at scan rates of (a) 5 mV/s and (b) 50 mV/s in 1 mM TEMPOL with 1 M NaCl solution. (c) Log(i_p) vs. log(v) graph highlighting the enhanced oxidation and reduction peak currents for the 10-dipped electrode, demonstrating optimal electron transfer and redox activity.*

Electrochemical Impedance Spectroscopy Analyses

EIS measurements were performed to assess ion transfer properties of the coated electrodes. Pristine, 1-dipped, 5-dipped and 10-dipped coated graphite felt electrodes were applied EIS tests after CV tests. Nyquist plots comparison of EIS results and the equivalent circuit are given

in Figure 5. Since this work focused only the effect of coating on electrodes, the comparison of their electrochemical behaviors observed by only the semi-circle part of the Nyquist graph. The differences of the semicircles between the specimens are remarkable. The element values of equivalent circuit are given in Table 2. CPE1 is the constant phase element (CPE), R_s is the solution resistance, and R_p is the polarization resistance which is the charge transfer resistance between electrodes and the electrolyte. R_p of 5-dipped electrodes have the lowest impedance value. Charge transfer resistance is related with the ion transfer between electrode surface and electrolyte, so it is affected from the electrode surface morphology [32,33]. Hence, due to the impedance of 5-dipped coated graphite felts lower than the other felts, it affected positively to the electrochemical properties. It is also observed that R_p of 10-dipped felt higher than all the other felts, which means that ion transfer is harder. The 5-dipped electrode CPE1 value is the highest, and 10-dipped electrode's is the second highest value in all electrodes. CPE is related to capacitance of electrodes and graphene coating improves the capacity of electrodes [34]. Error statistics and Kramers-Kronig values validate the EIS tests [35]. Nyquist plots (Figure 5) reveal that the 5-dipped electrodes achieved the lowest Rp value, indicating optimal ion transfer and surface morphology. While increasing dips to 5 improved electrode kinetics by enhancing the graphene-electrolyte interface, additional dips (10) slightly increased R_p, likely due to excessive coating thickness hindering ion transfer. [31]. Previous studies have shown that beyond a certain threshold, the addition of graphene negatively affects ion transfer. In this study, we found that the optimal threshold is 5- dips for EIS tests [19].

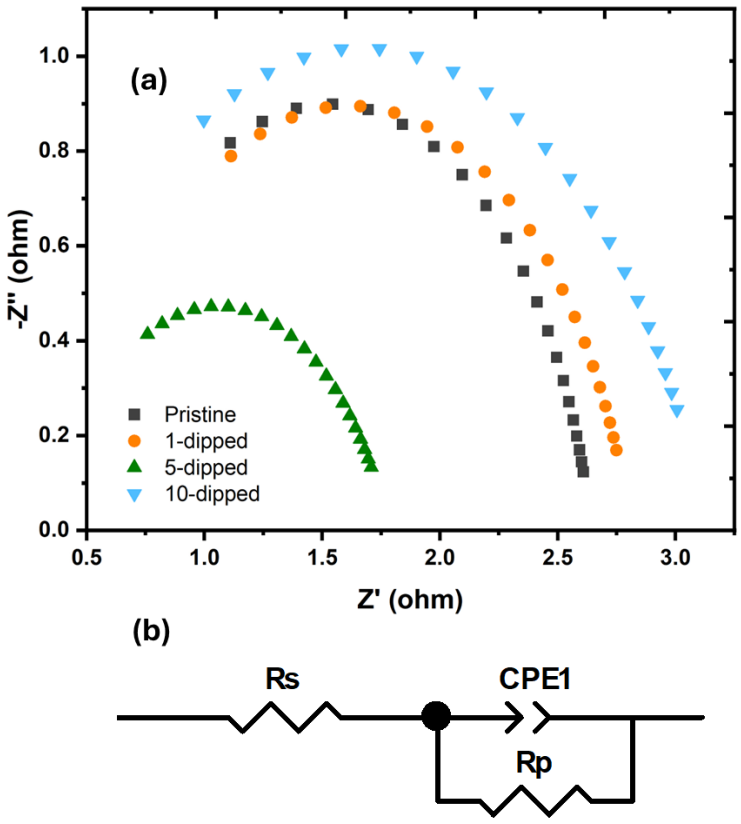

Figure 5. (a) Nyquist plots comparing the electrochemical impedance of pristine, 1-dipped, 5-dipped, and 10-dipped electrodes in a frequency range of 1 Hz to 10^5 Hz. (b) The equivalent

Randles circuit highlights the key elements influencing charge transfer and ion transport. Frequency range is from 1 Hz to 10^5 Hz, solution is 1 mM TEMPOL in 1 M NaCl. The 5-dipped electrode demonstrates the lowest polarization resistance, indicating optimal ion transfer due to improved electrode surface morphology.

Table 2. Equivalent circuit parameters derived from Nyquist plots, including R_s, R_p, and CPE1. The 5-dipped electrode exhibits the lowest R_p, indicating enhanced charge transfer efficiency compared to pristine and other dipped electrodes.

Element	Pristine	1-dipped	5-dipped	10-dipped
R_s (Ω)	0.4225	0.4209	0.3348	0.2077
R_p (Ω)	2.2200	2.3920	1.4480	2.9190
CPE1 ($\mu s^{\alpha}/\Omega$)	8.1440	15.7700	79.8300	24.9800
α	0.8669	0.8181	0.7364	0.7752
Error Statistics (X^2)	0.0184	0.0266	0.0291	0.0322
Kramers-Kronig (X^2)	$4.32x10^{-4}$	$6.09x10^{-4}$	$3.37x10^{-5}$	$5.36x10^{-4}$

XRD and Raman Analyses

Raman spectroscopy used to identify the characteristic bands of graphene, pristine and coated graphite felt and given Figure 6. The D-band indicates structural defects in carbon-based materials caused by impurity-induced lattice distortions. The doping effect, defects, number of graphene layers and stress are all indicated by the position and shape of the G band. The 2D band is the characteristic band of graphene, and the number of layers affects its shape. The LD/LG ratio is used to assess the purity of graphene, while the L_G/L_{2D} ratio is derived from the results of Raman spectroscopy to measure the total number of graphene layers. The research states that the L_D/L_G ratio should be between 0 and 1. The L_G/L_{2D} ratio for a single graphene was reported to be 0.25 in a recent work [36–38]. According to Raman spectroscopy results, D, G and 2D band are located at 1353 cm^{-1}, 1580 cm^{-1} and 2721 cm^{-1}, respectively for graphene. When L_D/L_G and L_G/L_{2D} ratios were calculated, it was determined that the graphene used in our study was of high purity and 6-7 layers.

Pristine and coated graphite felt's Raman spectroscopy results are given in Figure 6 (b). According to the results, all samples exhibit characteristic peaks for carbonaceous material, which is consistent with previous studies [39]. When the LD/LG ratios of the samples were examined, it was found that the highest ratio was in the pristine sample. This ratio decreased with the dipping process and the lowest ratio was obtained in the 10-dipped sample with 1.24. It is thought that as the number of dipping increases, more graphene is covered in the structure of the felt, resulting in this reduction. Furthermore, a peak attributed to C-H and C-H2 stretching and asymmetric stretching vibrations of the C-O-C glyco-sidic linkage of cellulose was found at the 1096 cm^{-1} location in the 5-dip sample [40,41].

Pristine, 5-dipped and 10-dipped graphite felt's XRD spectra are shown in Figure 6 (c). Two C peaks (Reference Code: ICDD 96-901-2231, hexagonal, a=b= 2.47 and c=6,7080) at 25.16° and 42.8° corresponding to the (100) and (104) crystal planes can be found from the XRD patterns of all specimens. The presence of any different phase in the coated samples was not

found due to the limitations of XRD identification. The XRD results obtained on the graphite felt compatible with the literature [18,42].

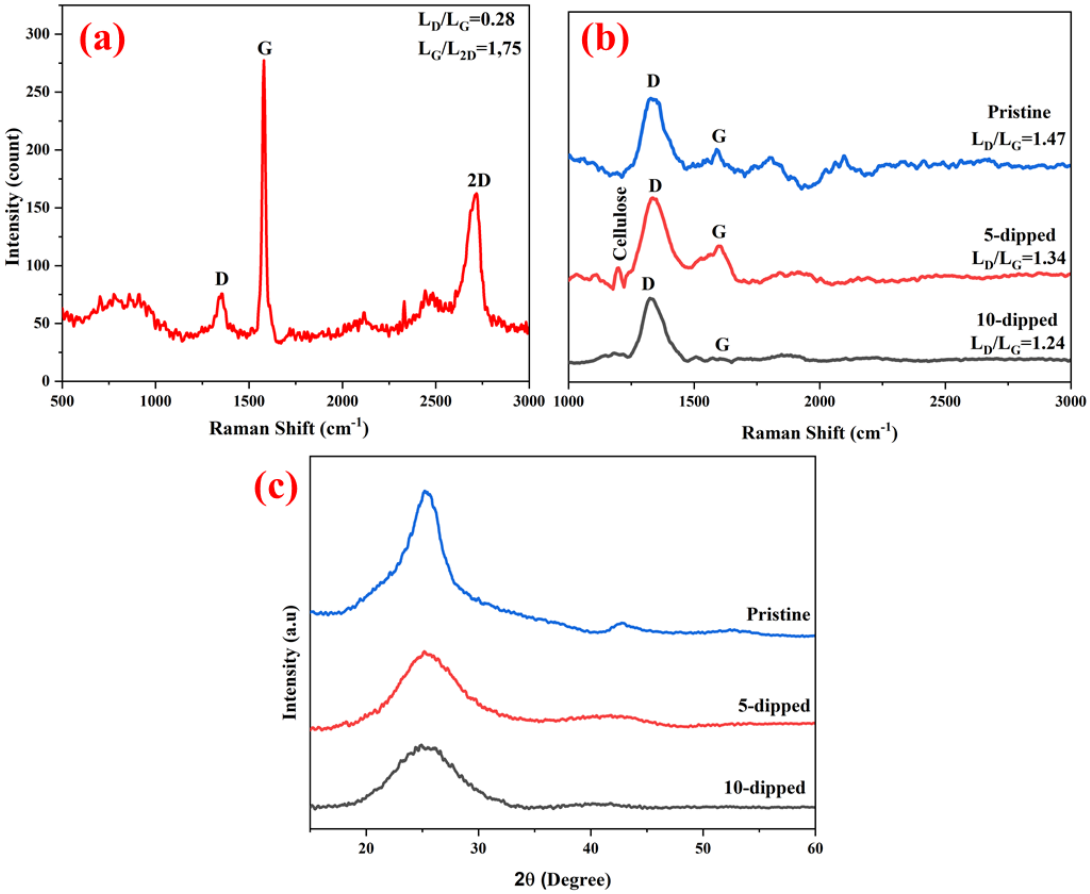

Figure 6. Raman spectroscopy results (a) graphene and (b) pristine, 5-dipped and 10 dipped graphite felt and (c) XRD result for all specimens.

Contact Angle Results

The effect of graphene coating on wettability properties of graphite felts observed with contact angle tests, which is shown in Figure 7 for pristine, 5-dipped and 10-dipped specimens. Distilled water dropped on the felts and contact angles were measured.

Pristine felt specimens have contact angles of approximately 155° on the left side and 159° on the right side, with an average contact angle of 157°. Since OFB applications need liquid electrolyte flowing in the cell, the electrodes of it should let liquid flowing. Graphene coating made the felt from hydrophobic to hydrophilic, which shows that coating affected positively to wettability.

Figure 7. The contact angle images of (a) pristine (b) 5-dipped (c) 10-dipped graphene coated felts. Dropped liquid is distilled water.

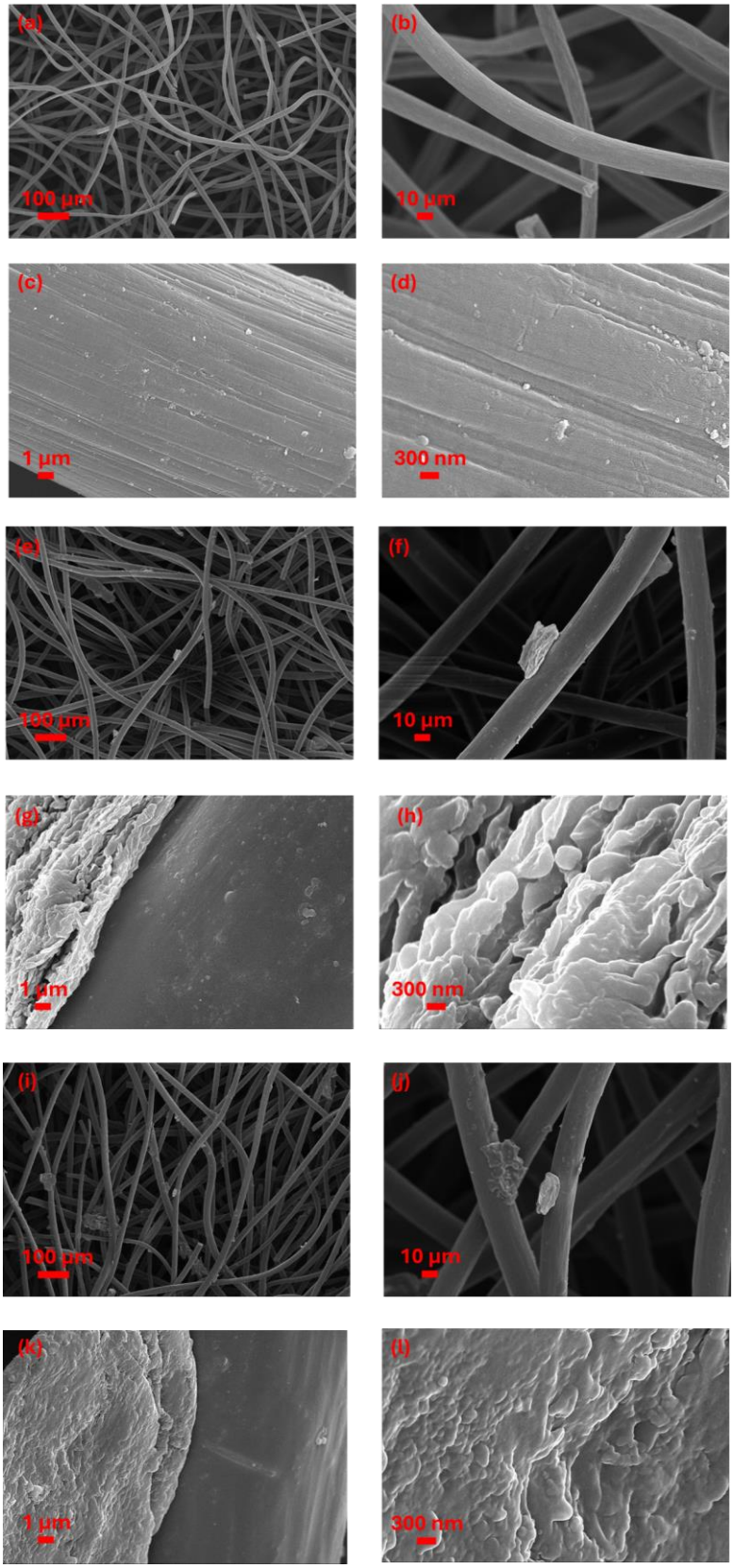

Figure 8. SEM images showing the surface morphologies of (a-d) pristine, (e-h) 5-dipped, and (i-l) 10-dipped graphite felts at magnifications of 100X, 500X, 5000X, and 20000X. The 5-dipped sample exhibits homogeneous graphene distribution, enhancing conductivity and electrochemical performance, while the 10-dipped sample shows stacked graphene layers, potentially reducing ion transfer efficiency due to increased thickness.

SEM Images

SEM analyses were done to observe the effect of coating on surface morphologies to electrodes, and images of pristine and 5- and 10-dipped coated graphite felts are given in **Hata! Başvuru kaynağı bulunamadı.**. Pristine graphite felt has a clean surface without any precipitation, which is shown in **Hata! Başvuru kaynağı bulunamadı.** Figure 8 (a) to (d). Graphene particles on the surface of 5-dipped graphite felt distributed homogeneously in **Hata! Başvuru kaynağı bulunamadı.** Figure 8 (e) to (h). In **Hata! Başvuru kaynağı bulunamadı.** Figure 8 (g), the graphene particle binds to the surface of a fiber of graphite felt clearly. In 10-dipped coated felt SEM images at **Hata! Başvuru kaynağı bulunamadı.** Figure 8 (i) to (l), graphene particles homogenously stacked onto the graphite felt fibers.

The pristine electrode exhibits a rough and irregular surface, characteristic of untreated graphite felt. At higher magnifications, the surface appears smooth but lacks any additional coating or modifications. This uncoated structure contributes to the hydrophobic nature of the pristine electrodes, as observed in the contact angle measurements. In contrast, the 5-dipped electrode shows a thin, uniform layer of graphene coating, effectively covering the surface while preserving the porosity of the felt. This uniformity enhances ion accessibility, contributing to the observed improvements in electrochemical performance. For the 10-dipped electrode, a thicker graphene layer is observed, with slight agglomeration in certain regions. While the increased graphene coverage provides more active sites for redox reactions, the reduced porosity may hinder ion transport, as indicated by the higher charge transfer resistance in EIS.

Redox Mechanism

The redox mechanism of the system is given in Figure 9. Dipping time effects the TEMPOL/TEMPOL$^+$ redox couple and increase the reduction and oxidation peaks. The improvement in electrochemical performance observed in this study can be attributed to the effects of graphene nanoplates followed by cellulose binders. The high electrical conductivity and large surface area of graphene facilitate efficient electron transfer and provide a large number of active sites for redox reactions of TEMPOL (Role of reduced graphene oxide as nano-electrocatalyst in carbon felt electrode of vanadium redox flow battery). As a binder, cellulose plays a role in maintaining electrode integrity and improving ion transport.

Electrochemical parameters from the literature are listed in Table 3. Since a scan rate of 50 mV/s and an electroactive material concentration of 1 mM were used in this study, the data have been normalized to these conditions. Most of the studies reviewed used vanadium as the electroactive material. Based on the peak current values, the results obtained in this study demonstrate comparable performance with other studies. Furthermore, consistent with a previous study [26], the dipping time has a positive effect on the peak current.

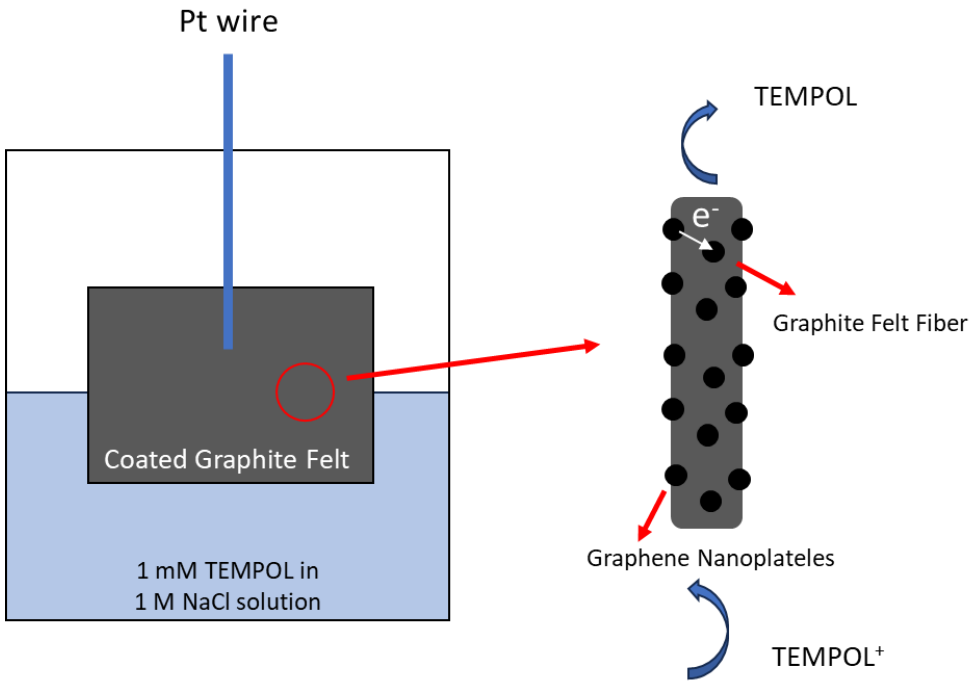

Figure 9. Mechanism of the electron transfer at the coated graphite felt.

Table 3. Comparison of electrochemical parameters derived from the CV curves of different studies. Peak currents are normalized to a scan rate of 50 mV/s and an electroactive material concentration of 1 mM. Differences in solvent molarity are not considered, assuming negligible impact on the electrochemical parameters.

Coating	Electroactive Material	Adhesion Material	Peak Potential (V)	Peak Current (mA/cm^2)	Study
Pristine	TEMPO	Ethylenediamine (EDA)	0.47 (0.68)	-1.399 (1.650)	[30]
GF-A (drying)			0.45 (0.71)	-5.948 (7.160)	
GF-B (microwave treatment)			0.38 (0.67)	-9.119 (9.817)	
Pristine	Vanadium	-	0.60 (1.2)	-1.900 (2.371)	[43]
Heat Treated			0.60 (1.21)	-2.060 (3.322)	
Vertical graphene			0.54 (1.22)	-4.667 (4.900)	
Nitrogen-functionalized vertical graphene			0.585 (1.19)	-4.590 (4.820)	
Pristine	Vanadium	Nafion	0.326 (0.470)	-2.370 (2.792)	[26]
5-dipped Graphene			0.345 (0.442)	-2.570 (2.664)	

10-dipped Graphene			0.339 (0.449)	-2.627 (2.827)	
Pristine	TEMPOL	Cellulose	0.74 (0.50)	-0.552 (0.828)	This Work
5-dipped Graphene			0.73 (0.50)	-0.828 (1.103)	
10-dipped Graphene			0.75 (0.50)	-1.379 (1.655)	

The comparative summary of the study is given in Table 4. According to EIS results, 5-dip electrode has higher ion transfer properties due to lower R_p. However, according to CV results, 10-dip electrode has higher oxidation and reduction peak currents and improved redox activity. This discrepancy is due to the interaction between ion transport efficiency and active site availability, as similarly discussed in studies comparing the complementary nature of EIS and CV techniques for analyzing electrochemical systems [44,45]. The thinner graphene coating on 5-dip electrode optimizes ion accessibility, while the thicker coating on 10-dip electrode maximizes the number of active sites for electron transfer. These findings indicate that electrode selection depends on specific application requirements that balance ion transport and electron transfer.

Table 4. Comparative summary of key electrochemical and surface performance measurements for pristine, 5-dip and 10-dip electrodes. The table includes oxidation and reduction peak currents from CV, polarization resistance from EIS, and contact angle measurements to assess wettability.

Parameter	Pristine	5-Dipped	10-Dipped
Oxidation Peak Current (mA)	0.828	1.103	1.655
Reduction Peak Current (mA)	-0.552	-0.828	-1.379
R_p (Ω)	2.2200	1.4480	2.9190
Contact Angle (°)	157°	0°	0°

Conclusion

This study presents the development of cellulose-bonded graphene nanoplatelet-coated electrodes with promising applications in renewable energy storage and grid-level systems. These electrodes demonstrate high electrochemical performance, combining the sustainability and cost-effectiveness of cellulose with the conductivity and structural benefits of graphene. The results highlight their potential as an alternative to costly materials like Nafion, particularly in TEMPOL-based organic flow batteries.

Key findings from this study include the significant enhancement in wettability and ion transport due to the graphene-cellulose composite, transforming the electrode surface from hydrophobic to hydrophilic. Surface characterization analyses—such as SEM imaging, Raman spectroscopy, and contact angle measurements—confirm these structural improvements. Furthermore, the electrochemical performance, as evaluated through CV and EIS, underlines

the importance of optimizing the dip-coating process. While the 5-dip coating demonstrated optimal ion transfer efficiency and lower charge transfer resistance, the 10-dip coating exhibited higher redox activity and oxidation-reduction peak currents.

Despite these advancements, certain limitations must be addressed to advance this technology toward commercialization. The scalability of the dip-coating method, particularly in achieving uniform coatings on large-scale electrodes, remains a challenge. Additionally, the long-term stability of cellulose as a binder under varied environmental and cycling conditions requires further investigation. The dip-coating method employed in this study provides a practical and adaptable approach to mass production, making these electrodes a viable candidate for industrial energy storage applications. By addressing the remaining challenges, this technology can contribute significantly to the global transition toward clean and sustainable energy systems, demonstrating the transformative potential of cellulose-bonded graphene electrodes in the energy storage.

Author Contributions

T.Y. Eken: data curation, formal analysis, investigation, methodology, validation, visualization, writing – original draft, writing – review & editing
C. Kaykılarlı: data curation, formal analysis, methodology, validation, visualization, writing – original draft, writing – review & editing
A. Tuna: data curation, formal analysis, methodology, validation, visualization, writing – original draft, writing – review & editing
E.D. Şam Parmak: Supervision, validation, writing – review & editing
D. Uzunsoy: Resources, supervision, validation, writing – review & editing
P. Peljo: Resources, supervision, methodology, validation, visualization, writing – review & editing

Conflicts of interest

All authors read and commented on the manuscript and have no conflicts of interest to declare.

Acknowledgements

We would like to thank to Bursa Technical University (Türkiye), University of Turku (Finland) and Aalto University (Finland) for their unconditional supports. TYE and DU also would like to thank to Bursa Technical University Scientific Research Projects Coordinatorship for the project number 210D005. TYE also would like to thank to Erasmus+, Turkish National Agency, and Bursa Technical University Erasmus Office for the Erasmus+ funding.

References

[1] Huskinson B, Marshak MP, Suh C, Er S, Gerhardt MR, Galvin CJ, et al. A metal-free organic–inorganic aqueous flow battery. Nature 2014;505:195–8. https://doi.org/10.1038/nature12909.
[2] Beh ES, De Porcellinis D, Gracia RL, Xia KT, Gordon RG, Aziz MJ. A Neutral pH Aqueous Organic–Organometallic Redox Flow Battery with Extremely High Capacity

Retention. ACS Energy Lett 2017;2:639–44. https://doi.org/10.1021/acsenergylett.7b00019.
[3] Chen Q, Li Y, Liu Y, Sun P, Yang Z, Xu T. Designer Ferrocene Catholyte for Aqueous Organic Flow Batteries. ChemSusChem 2021;14:1295–301. https://doi.org/10.1002/cssc.202002467.
[4] Cao J, Tian J, Xu J, Wang Y. Organic Flow Batteries: Recent Progress and Perspectives. Energy Fuels 2020;34:13384–411. https://doi.org/10.1021/acs.energyfuels.0c02855.
[5] Liu Y, Chen Q, Sun P, Li Y, Yang Z, Xu T. Organic electrolytes for aqueous organic flow batteries. Materials Today Energy 2021;20:100634. https://doi.org/10.1016/j.mtener.2020.100634.
[6] Yang B, Hoober-Burkhardt L, Krishnamoorthy S, Murali A, Prakash GKS, Narayanan SR. High-Performance Aqueous Organic Flow Battery with Quinone-Based Redox Couples at Both Electrodes. J Electrochem Soc 2016;163:A1442. https://doi.org/10.1149/2.1371607jes.
[7] Schwenke AM, Janoschka T, Stolze C, Martin N, Hoeppener S, Schubert US. Microwave-assisted preparation of carbon nanofiber-functionalized graphite felts as electrodes for polymer-based redox-flow batteries. Journal of Power Sources 2016;335:155–61. https://doi.org/10.1016/j.jpowsour.2016.09.121.
[8] Yang B, Wang Z, Wang W, Lu Y-C. A Low-Crossover and Fast-Kinetics Thiolate Negolyte for Aqueous Redox Flow Batteries. Energy Material Advances 2022;2022. https://doi.org/10.34133/2022/9795675.
[9] Mousavihashemi S, Murcia-López S, Hosseini MG, Morante JR, Flox C. Towards Production of a Highly Catalytic and Stable Graphene-Wrapped Graphite Felt Electrode for Vanadium Redox Flow Batteries. Batteries 2018;4:63. https://doi.org/10.3390/batteries4040063.
[10] Anantha MS, Anarghya D, Hu C, Reddy N, Venkatesh K, Muralidhara HB. Electrochemical performance of graphene oxide modified graphite felt as a positive electrode in all-iron redox flow batteries. J Appl Electrochem 2021;51:331–44. https://doi.org/10.1007/s10800-020-01490-5.
[11] Park M, Ryu J, Wang W, Cho J. Material design and engineering of next-generation flow-battery technologies. Nat Rev Mater 2016;2:1–18. https://doi.org/10.1038/natrevmats.2016.80.
[12] Zhao Q, Zhu Z, Chen J. Molecular Engineering with Organic Carbonyl Electrode Materials for Advanced Stationary and Redox Flow Rechargeable Batteries. Advanced Materials 2017;29:1607007. https://doi.org/10.1002/adma.201607007.
[13] Nie CT, Han HJ, Li YH, Zheng SH, Wang Y. Porous Graphite Felt Modified with Carbon Nanoparticles for an MV/4-HO-TEMPO Flow Battery. ACS Appl Nano Mater 2024;7:9950–9. https://doi.org/10.1021/acsanm.3c06270.
[14] Wang D, Xu Z, Zhao H, Li X, Qin X, Song Z, et al. Conductivity and adsorbability synergistically improved electrode for high-performance viologen based aqueous organic flow batteries. Chemical Engineering Journal 2024;479:147799. https://doi.org/10.1016/j.cej.2023.147799.
[15] Gao F, Cai X, Huang C. The impact of modified electrode on the performance of an DHAQ/ K4Fe(CN)6 redox flow battery. Electrochimica Acta 2021;390:138847. https://doi.org/10.1016/j.electacta.2021.138847.
[16] Zhang Y, Liu W, Wang Z, Shen Y-M, Wang W, Chen Z, et al. Tetrapyridophenazine/graphene composites for aqueous hybrid flow battery anodes with long cycle life. Carbon 2020;161:309–15. https://doi.org/10.1016/j.carbon.2020.01.092.

[17] Cao J, Zhu Z, Xu J, Tao M, Chen Z. Nitrogen-doped porous graphene as a highly efficient cathodic electrocatalyst for aqueous organic redox flow battery application. J Mater Chem A 2017;5:7944–51. https://doi.org/10.1039/C7TA00873B.
[18] Liu T, Li X, Nie H, Xu C, Zhang H. Investigation on the effect of catalyst on the electrochemical performance of carbon felt and graphite felt for vanadium flow batteries. Journal of Power Sources 2015;286:73–81. https://doi.org/10.1016/j.jpowsour.2015.03.148.
[19] Loghavi MM, Zarei-Jelyani M, Babaiee M, Niknam Z, Eqra R. Graphene/Nafion ink-impregnated graphite felt for both positive and negative sides of enhanced vanadium redox flow battery. J Solid State Electrochem 2023;27:2237–50. https://doi.org/10.1007/s10008-023-05476-z.
[20] Ji J, Noh C, Shin M, Oh S, Chung Y, Kwon Y, et al. Vanadium redox flow batteries using new mesoporous nitrogen-doped carbon coated graphite felt electrode. Applied Surface Science 2023;611:155665. https://doi.org/10.1016/j.apsusc.2022.155665.
[21] Li Z, Yang W, Bao J, Kong Y, Jing S, Zhang J, et al. Reduced graphene oxide/MXene hybrid decorated graphite felt as an effective electrode for vanadium redox flow battery. RSC Advances 2024;14:12158–70. https://doi.org/10.1039/D4RA01306A.
[22] Bellani S, Najafi L, Prato M, Oropesa-Nuñez R, Martín-García B, Gagliani L, et al. Graphene-Based Electrodes in a Vanadium Redox Flow Battery Produced by Rapid Low-Pressure Combined Gas Plasma Treatments. Chem Mater 2021;33:4106–21. https://doi.org/10.1021/acs.chemmater.1c00763.
[23] Sankar A, Michos I, Dutta I, Dong J, Angelopoulos AP. Enhanced vanadium redox flow battery performance using graphene nanoplatelets to decorate carbon electrodes. Journal of Power Sources 2018;387:91–100. https://doi.org/10.1016/j.jpowsour.2018.03.045.
[24] Weng Z, Su Y, Wang D-W, Li F, Du J, Cheng H-M. Graphene–Cellulose Paper Flexible Supercapacitors. Advanced Energy Materials 2011;1:917–22. https://doi.org/10.1002/aenm.201100312.
[25] Tang Y, He Z, Mosseler JA, Ni Y. Production of highly electro-conductive cellulosic paper via surface coating of carbon nanotube/graphene oxide nanocomposites using nanocrystalline cellulose as a binder. Cellulose 2014;21:4569–81. https://doi.org/10.1007/s10570-014-0418-9.
[26] Di Virgilio M, Basso Peressut A, Arosio V, Arrigoni A, Latorrata S, Dotelli G. Functional and Environmental Performances of Novel Electrolytic Membranes for PEM Fuel Cells: A Lab-Scale Case Study. Clean Technologies 2023;5:74–93. https://doi.org/10.3390/cleantechnol5010005.
[27] Gallo Stampino P, Riva L, Punta C, Elegir G, Bussini D, Dotelli G. Comparative Life Cycle Assessment of Cellulose Nanofibres Production Routes from Virgin and Recycled Raw Materials. Molecules 2021;26:2558. https://doi.org/10.3390/molecules26092558.
[28] Zhao D, Zhu Y, Cheng W, Chen W, Wu Y, Yu H. Cellulose-Based Flexible Functional Materials for Emerging Intelligent Electronics. Advanced Materials 2021;33:2000619. https://doi.org/10.1002/adma.202000619.
[29] Wan C, Jiao Y, Li J. Flexible, highly conductive, and free-standing reduced graphene oxide/polypyrrole/cellulose hybrid papers for supercapacitor electrodes. J Mater Chem A 2017;5:3819–31. https://doi.org/10.1039/C6TA04844G.
[30] Li X, Huang C. A new modification method for graphite felt electrodes in a MV/4-HO-TEMPO flow battery. RSC Advances 2020;10:6333–41. https://doi.org/10.1039/C9RA10966H.
[31] Xia L, Zhang Q, Wu C, Liu Y, Ding M, Ye J, et al. Graphene coated carbon felt as a high-performance electrode for all vanadium redox flow batteries. Surface and Coatings Technology 2019;358:153–8. https://doi.org/10.1016/j.surfcoat.2018.11.024.

[32] Zhang Y, Qian G, Huang C, Wang Y. Effect of modification of polyacrylonitrile-based graphite felts on their performance in redox fuel cell and redox flow battery. Journal of Power Sources 2016;324:528–37. https://doi.org/10.1016/j.jpowsour.2016.05.115.
[33] Shobukawa H, Alvarado J, Yang Y, Meng YS. Electrochemical performance and interfacial investigation on Si composite anode for lithium ion batteries in full cell. Journal of Power Sources 2017;359:173–81. https://doi.org/10.1016/j.jpowsour.2017.05.044.
[34] Brug GJ, van den Eeden ALG, Sluyters-Rehbach M, Sluyters JH. The analysis of electrode impedances complicated by the presence of a constant phase element. Journal of Electroanalytical Chemistry and Interfacial Electrochemistry 1984;176:275–95. https://doi.org/10.1016/S0022-0728(84)80324-1.
[35] Boukamp BA. A Linear Kronig-Kramers Transform Test for Immittance Data Validation. J Electrochem Soc 1995;142:1885. https://doi.org/10.1149/1.2044210.
[36] Wu Y, Wang B, Ma Y, Huang Y, Li N, Zhang F, et al. Efficient and large-scale synthesis of few-layered graphene using an arc-discharge method and conductivity studies of the resulting films. Nano Res 2010;3:661–9. https://doi.org/10.1007/s12274-010-0027-3.
[37] Kaykılarlı C, Uzunsoy D, Parmak EDŞ, Fellah MF, Çakır ÖÇ. Boron and nitrogen doping in graphene: an experimental and density functional theory (DFT) study. Nano Ex 2020;1:010027. https://doi.org/10.1088/2632-959X/ab89e9.
[38] Cotul U, Parmak E, Kaykilarli C, Saray O, Colak Ö, Uzunsoy D. Development of High Purity, Few-Layer Graphene Synthesis by Electric Arc Discharge Technique. ACTA PHYSICA POLONICA A 2018;134. https://doi.org/10.12693/aphyspola.134.289.
[39] Zhou L, Zhou M, Hu Z, Bi Z, Serrano KG. Chemically modified graphite felt as an efficient cathode in electro-Fenton for *p*-nitrophenol degradation. Electrochimica Acta 2014;140:376–83. https://doi.org/10.1016/j.electacta.2014.04.090.
[40] Agarwal UP, Ralph SA, Baez C, Reiner RS. Detection and quantitation of cellulose II by Raman spectroscopy. Cellulose 2021;28:9069–79. https://doi.org/10.1007/s10570-021-04124-x.
[41] Satha H, Kouadri I, Benachour D. Thermal, Structural and Morphological Studies of Cellulose and Cellulose Nanofibers Extracted from Bitter Watermelon of the Cucurbitaceae Family. J Polym Environ 2020;28:1914–20. https://doi.org/10.1007/s10924-020-01735-6.
[42] Lee W-J, Wu Y-T, Liao Y-W, Liu Y-T. Graphite Felt Modified by Atomic Layer Deposition with TiO2 Nanocoating Exhibits Super-Hydrophilicity, Low Charge-Transform Resistance, and High Electrochemical Activity. Nanomaterials 2020;10:1710. https://doi.org/10.3390/nano10091710.
[43] Guo J, Pan L, Sun J, Wei D, Dai Q, Xu J, et al. Metal-free Fabrication of Nitrogen-doped Vertical Graphene on Graphite Felt Electrodes with Enhanced Reaction Kinetics and Mass Transport for High-performance Redox Flow Batteries. Advanced Energy Materials 2024;14:2302521. https://doi.org/10.1002/aenm.202302521.
[44] Randviir EP. A cross examination of electron transfer rate constants for carbon screen-printed electrodes using Electrochemical Impedance Spectroscopy and cyclic voltammetry. Electrochimica Acta 2018;286:179–86. https://doi.org/10.1016/j.electacta.2018.08.021.
[45] Gharbi O, Tran MTT, Tribollet B, Turmine M, Vivier V. Revisiting cyclic voltammetry and electrochemical impedance spectroscopy analysis for capacitance measurements. Electrochimica Acta 2020;343:136109. https://doi.org/10.1016/j.electacta.2020.136109.